

## X-Ray Photoelectron Study of the Valence Bands in Cuprous Halides

S. Kono, T. Ishii, T. Sagawa, and T. Kobayasi

*Department of Physics, Tohoku University, Sendai, Japan*

(Received 23 January 1973)

The x-ray photoelectron spectra of the valence bands of CuCl, CuBr, and CuI have been measured. The spectra show that the valence bands of these materials consist of two branches. The existence of a forbidden band between the two branches and a few additional structures are revealed by the deconvolution of the spectra with a measured instrumental response function. The average  $p$ - $d$  mixing rates in the valence bands are evaluated by taking the transition matrix elements into account. It is shown that the upper branch of the valence bands arises mostly from the  $3d$  states of a cuprous ion, in accordance with the optical-absorption spectra in the ultraviolet region. The results are compared with other experimental and theoretical data. Especially, the fundamental absorption spectra are reinterpreted.

### I. INTRODUCTION

The optical properties of cuprous halides, for example, the photoabsorption and the luminescence due to high-density excitons, have been the subject of extensive study. However, only a few works<sup>1-7</sup> have been carried out from the viewpoint of the investigation of the energy-band structure. Semiconductors with the zinc-blende or diamond crystal structure form an isoelectronic sequence beginning with a covalent material in the fourth column of the Periodic Table and ending with a I-VII compound,<sup>2</sup> such as Ge, GaAs, ZnSe, and CuBr. The band gaps of the materials in this sequence except cuprous halides change according to a quadratic dependence on the deviation of the valence number from that of the material in the fourth column. The band-gap energy of a cuprous halide estimated from the location of the exciton band in the fundamental absorption spectrum is smaller than the value expected from this quadratic dependence. The exciton absorption is not intense and the absorption intensity is weak in the region between the exciton band and the third peak.<sup>3</sup> The strong absorption peaks occur in the energy region more than a few electron volts above the threshold. The spin-orbit splitting of the exciton band is small in CuBr and CuI as compared with the values expected from the splitting in respective halogen ions, and is inverted in CuCl.<sup>4,5</sup> All of these aspects of the optical spectra of cuprous halides have been ascribed to the  $3d$  states of the  $\text{Cu}^+$  ion being the majority in the upper part of the valence band in contrast with the case of other materials in the isoelectronic sequence. The band calculation by Song<sup>6</sup> is consistent with this interpretation, at least in a qualitative manner. A remarkable feature of the calculated band structure is the presence of a forbidden band between the  $d$ -rich upper valence band and the  $p$ -rich lower valence band, as first suggested by Herman and McClure.<sup>7</sup>

The photoelectron measurement is quite suitable for obtaining informations on the valence band. In particular, x-ray photoelectron spectroscopy (XPS)<sup>8</sup> has certain advantages as compared with ultraviolet photoelectron spectroscopy (UPS).<sup>8</sup> Because of the high energy of the incident x-ray photon, the electron is excited to a state almost monotonic and structureless in its energy dependence. Electrons inelastically scattered in the course of the transport to the surface give rise to only a small structureless background in the region of the valence-band spectrum. Such a contribution from scattered electrons can be subtracted from the spectrum. The potential barrier at the surface has no important effect on the escape of photoexcited electrons with an energy of the order of  $10^3$  eV. Thus, the valence-band spectrum is determined mostly by the density of states of the valence band and the transition matrix elements between the valence states and the high-energy conduction states. On the other hand, the instrumental resolution which is mainly governed by the natural width of exciting light is not high enough to resolve the details of the valence band. In the present case, where a measuring system with an x-ray monochromator is not available, the deconvolution of the measured spectrum with an appropriate response function should be made for supplementing the low resolution.

The purpose of the present paper is to describe an XPS study of the nature of the valence bands in cuprous halides. We will show a direct evidence for the existence of the forbidden band between the two valence bands and estimate the average  $p$ - $d$  mixing rate in each band. The experimental procedure and the results are described in Secs. II and III, respectively. Section IV is devoted to evaluate the average  $p$ - $d$  mixing rates in the valence bands. In Sec. V, the discussion of the results is given along with the comparison with other experi-

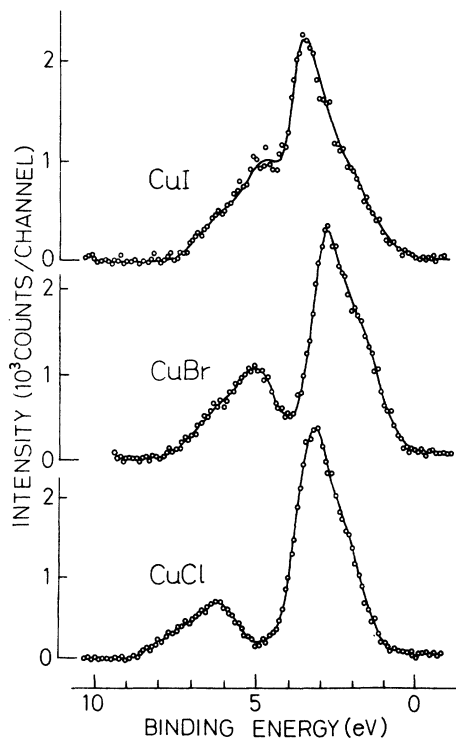


FIG. 1. X-ray photoelectron spectra for the valence bands of CuCl, CuBr, and CuI.

mental and theoretical data, and the fundamental absorption spectra are reinterpreted.

## II. EXPERIMENTAL PROCEDURE

An electron energy analyzer of the hemispherical-electrostatic-condenser type with 51-mm mean radius was constructed and used for the measurements. Both  $MgK_{\alpha}$  (1253.6 eV) and  $AlK_{\alpha}$  (1486.6 eV) radiations were used for excitation. The x-ray tube was usually operated at 7 kV and 100 mA. A retarding voltage of about 800 V was applied to a sample holder in the case of the measurement of the valence-band spectra. The resolution in this case, estimated from the full width at half-maximum of the  $Au N_7$  line, was 1.0 eV for  $MgK_{\alpha}$  excitation. The scanning was carried out by changing the retarding voltage, and the output counts were stored in a 1000-channel multiscaler by repeating the scanning.

Samples were prepared by evaporation *in situ* onto the stainless-steel sample holder at  $2 \sim 4 \times 10^{-6}$  Torr. The starting materials were chemically purified and zone refined.<sup>9</sup> The samples of CuI were prepared by evaporation onto the sample holder heated at about 150 °C, so that the samples with the zinc-blende-type crystal structure were obtained.<sup>4</sup> For CuCl and CuBr, such a heating was not necessary. Novakov<sup>10</sup> reported that satellite bands associated with the copper 2p lines were

found in the spectrum of CuCl, and later related it to the adsorption of water or oxygen. No satellite band of this kind was found to occur in the present experiment. This kind of discrepancy may often be caused by the difference of the sample preparation. CuCl changes its chemical state upon exposure to air and this is recognized by the change of its color. In order to examine the difference of the XPS spectrum due to the difference of the chemical state, the copper 2p lines of  $CuCl_2 \cdot 2H_2O$  were measured. In this case, the satellite bands were found. This suggests that the satellite is inherent in the cupric ion, not in the cuprous ion. Recently, Frost *et al.*<sup>11</sup> have carried out an extensive study on cupric and cuprous compounds and confirmed that the satellite of the copper 2p line is characteristic of the  $Cu^{2+}$  ion. Since no satellite of the  $Cu^{2+}$  2p line was observed in the present experiment, the XPS spectra obtained here give those of cuprous halides free from oxidation or adsorption of water.

Since a nonmetallic sample is charged during x-ray irradiation, the binding energy should be carefully determined so that the charging effect is eliminated. The electron energy analyzer was calibrated with the high-energy edge of the valence-band spectrum of Pd metal.<sup>12</sup> Binding energies were determined by the comparison with the energy of the 3d line of Ag metal, which was evaporated onto a cuprous halide sample. The location of the Fermi level of a cuprous halide thus determined seems to still contain a little inaccuracy.

## III. EXPERIMENTAL RESULTS

Figure 1 shows the photoelectron spectra of the valence bands of CuCl, CuBr, and CuI obtained by  $MgK_{\alpha}$  irradiation. The abscissa is the binding energy and the ordinate is the intensity. The counting time for one channel was 120 sec for CuCl and CuBr, and 180 sec for CuI. The spectral resolution is 1.0 eV for all materials.

Each spectrum is composed of two bands. The upper band appears to have composite structure which is not clearly resolved. Because of the natural width of  $MgK_{\alpha}$  radiation, the bands occurring in the spectra are much more broadened than the widths of the valence bands. Therefore, the spectra of CuCl and CuBr strongly suggest the existence of a forbidden band between the upper and lower bands.

The spectra shown in Fig. 1, were deconvoluted by a modified Gauss-Seidel method.<sup>13</sup> In order to avoid the occurrence of spurious unphysical structures, an ordinary smoothing procedure was inserted before each iteration. The spectral profile of the  $Au 4f (N_7)$  line was measured and used as the response function. Small unphysical oscillations occurring in the deconvoluted curve were excluded

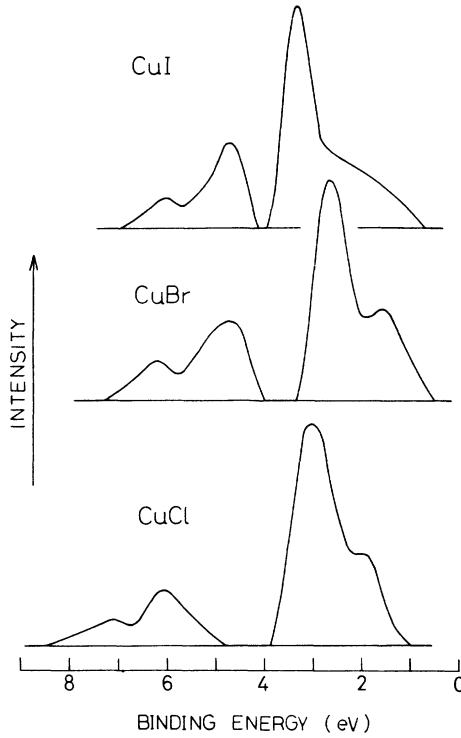


FIG. 2. Deconvoluted XPS spectra obtained from the spectra given in Fig. 1 by a modified Gauss-Seidel method with 100-times iteration.

in such a manner as not to change the total area under the obtained curve. This did not change the detail of the major profile of the obtained spectrum. In addition to this, a few known test functions were deconvoluted and the validity of the procedure was confirmed. Figure 2 shows the deconvoluted spectra of the valence bands. The spectra indicate the existence of the forbidden band in all of the three materials. The composite structures in the upper bands in Fig. 1 are more clearly resolved, and structures are also revealed in the lower bands. The gaps between the upper and lower bands of CuCl, CuBr, and CuI decrease in that order.

In order to see the dependence of the spectral profile on the exciting photon energy, the valence-band spectra were observed by the excitation with  $AlK_{\alpha}$  radiation, whose energy is more than 200 eV higher than that of  $MgK_{\alpha}$  radiation. The instrumental resolution was adjusted to be the same in both cases. The obtained spectra were the same in their spectral profiles as those obtained with  $MgK_{\alpha}$  radiation. This result indicates no dependence of the XPS spectrum under question on the exciting photon energy, and from this we may conclude that the excited state for the photoelectron is monotonic and structureless as mentioned in Sec. I.

#### IV. EVALUATION OF THE AVERAGE $p$ - $d$ MIXING RATES

The magnitudes of the average  $p$ - $d$  mixing rates in the valence bands can be evaluated from the analysis of the spectra given in Fig. 2. In this analysis, the ratio, denoted as  $R$  hereafter, of the integrated intensity of the upper band to that of the lower band in the XPS spectrum plays an important role. As is mentioned in Sec. I, the scattering and escape processes are unimportant in the present case. Thus, the photoelectron spectrum is given by

$$N_{\lambda}(E, \hbar\omega) = A \sum_{\mathbf{k}, i} |(\Psi_{c\mathbf{k}} | \nabla | \Psi_{\lambda i\mathbf{k}})|^2 \times \delta(E_{c\mathbf{k}} - E_{\lambda i\mathbf{k}} - \hbar\omega) \delta(E - E_{\lambda i\mathbf{k}}), \quad (1)$$

where  $\lambda$  distinguishes the upper ( $\lambda = u$ ) and lower ( $\lambda = l$ ) valence bands,  $\Psi_{\lambda i\mathbf{k}}$  is the wave function of an electron in the  $i$ th component band of the  $\lambda$  valence band with energy  $E_{\lambda i\mathbf{k}}$ ,  $\Psi_{c\mathbf{k}}$  the wave function of an electron excited to a conduction state with high energy  $E_{c\mathbf{k}}$ , and  $A$  a constant. The dipole transition approximation is used since the multipole expansion parameter is very small in the present case. The summation over the initial-state wave vector in the reduced zone is replaced by that over the final-state wave vector in the extended zone. It is assumed that the valence states can be described in terms of the tight-binding approximation, and  $\Psi_{c\mathbf{k}}$  can be described by a single plane wave orthogonalized to the valence and core states (SOPW). The energy of the excited electron is approximated as  $E_{c\mathbf{k}} = E_{c0} + \hbar^2 k^2 / 2m$ . Since the energy dispersions of the valence states are negligibly small as compared with the excitation energy,  $R$  can be written as

$$R = \frac{\int dE N_u(E, \hbar\omega)}{\int dE N_l(E, \hbar\omega)} = \frac{\sum_{i=1}^{n_u} \int d\Omega_{\mathbf{k}} |(\Psi_{c\mathbf{k}} | \nabla | \Psi_{u i\mathbf{k}})|^2}{\sum_{i=1}^{n_l} \int d\Omega_{\mathbf{k}} |(\Psi_{c\mathbf{k}} | \nabla | \Psi_{l i\mathbf{k}})|^2} \quad (d\Omega_{\mathbf{k}} = \sin\theta_{\mathbf{k}} d\theta_{\mathbf{k}} d\varphi_{\mathbf{k}}). \quad (2)$$

Here,  $n_{\lambda}$  is the number of the component bands in the  $\lambda$  valence band,  $k = [2m\hbar^{-2}(\hbar\omega + E_{ui} - E_{c0})]^{1/2}$ , and  $k' = [2m\hbar^{-2}(\hbar\omega + E_{li} - E_{c0})]^{1/2}$ . In practice one can put  $k = k'$ . In the tight-binding approximation,  $\Psi_{\lambda i\mathbf{k}}$  is given by

$$\Psi_{\lambda i\mathbf{k}}(\mathbf{r}) = N^{-1/2} \sum_{\mu, \alpha, j} C_{\lambda i\mathbf{k}}^{\mu, \alpha} e^{i\mathbf{k} \cdot \mathbf{R}_j} \phi_{\mu, \alpha}(\mathbf{r} - \mathbf{R}_j), \quad (3)$$

where  $\phi_{\mu, \alpha}$  is an ionic orbital,  $\mu$  ( $= Cu^+$  or  $X^-$ ) distinguishes the copper and halogen ions,  $\alpha$  [ $= (n, l, m)$ ] stands for the quantum number of the  $Cu^+$   $3d$  and the outermost  $X^-$   $np$  orbitals, and  $N$  is the number of unit cells in the crystal. The summation

over  $j$  is taken over the  $\mu$ -type sublattice. The overlap integrals between the ionic orbitals on different sites are neglected, so that the Bloch sums,  $N^{-1/2} \sum_j e^{i\vec{k} \cdot \vec{R}_j} \phi_{\mu, \alpha}(\vec{r} - \vec{R}_j)$ , form an orthonormal set. In practice,  $\Psi_{c\vec{k}}$  is well approximated by a plane wave orthogonalized only to all of the core and valence-band Bloch sums.

The expansion coefficients  $C_{\lambda i \vec{k}}^{\mu, \alpha}$  determine the properties of the  $p$ - $d$  mixing in the upper and lower valence bands. If the matrix elements between the ionic orbitals on different sites appearing through the orthogonalization terms are neglected, the matrix elements in Eq. (2) become

$$(\Psi_{c\vec{k}} | \nabla | \Psi_{\lambda i \vec{k}}) = \sum_{\mu, \alpha} C_{\lambda i \vec{k}}^{\mu, \alpha} (\phi_{c\vec{k}, \mu} | \nabla | \phi_{\mu, \alpha}), \quad (4)$$

where  $\phi_{c\vec{k}, \mu}$  is a single plane wave orthogonalized to the  $\mu$ -type ionic orbitals and has the normalization factor of  $\Psi_{c\vec{k}}$ .

Suppose that the spherical energy surface of the excited electron in the extended zone is folded into the reduced zone. Since the original spherical surface has very large value of  $k$ , the folded surface distributes throughout the first Brillouin zone so complicatedly that the coefficient  $C_{\lambda i \vec{k}}^{\mu, \alpha}$  varies rapidly and almost randomly when  $\vec{k}$  runs over the original spherical surface. On the other hand,  $(\phi_{c\vec{k}, \mu} | \nabla | \phi_{\mu, \alpha})^* (\phi_{c\vec{k}, \mu'} | \nabla | \phi_{\mu', \alpha'})$  varies rather monotonically. Thus,  $(C_{\lambda i \vec{k}}^{\mu, \alpha})^* C_{\lambda i \vec{k}}^{\mu', \alpha'}$  can be replaced by its average  $\langle (C_{\lambda i \vec{k}}^{\mu, \alpha})^* C_{\lambda i \vec{k}}^{\mu', \alpha'} \rangle_{av}$ , in the first Brillouin zone, in carrying out the integration. For the orbitals under consideration, the integral  $\int d\Omega_{\vec{k}} (\phi_{c\vec{k}, \mu} | \nabla | \phi_{\mu, \alpha})^* (\phi_{c\vec{k}, \mu'} | \nabla | \phi_{\mu', \alpha'})$  vanishes except for  $(\mu, \alpha) = (\mu', \alpha')$ . Thus, from Eq. (4) the integration over  $\Omega_{\vec{k}}$  is written as

$$\int d\Omega_{\vec{k}} |(\Psi_{c\vec{k}} | \nabla | \Psi_{\lambda i \vec{k}})|^2 = \sum_{\mu, \alpha} \langle |C_{\lambda i \vec{k}}^{\mu, \alpha}|^2 \rangle_{av} \times \int d\Omega_{\vec{k}} |(\phi_{c\vec{k}, \mu} | \nabla | \phi_{\mu, \alpha})|^2. \quad (5)$$

Since the  $\Omega_{\vec{k}}$  integral of  $|(\phi_{c\vec{k}, \mu} | \nabla | \phi_{\mu, \alpha})|^2$  is independent of the quantum number  $m$ , the ratio  $R$  is given from Eqs. (2) and (5) as

$$R = n_u (\gamma p_u + d_u) / n_l (\gamma p_l + d_l), \quad (6)$$

where

$$p_\lambda = n_\lambda^{-1} \sum_{i=1}^{n_\lambda} \sum_{m=-1}^1 \langle |C_{\lambda i \vec{k}}^{pm}|^2 \rangle_{av}, \quad (7)$$

$$d_\lambda = n_\lambda^{-1} \sum_{i=1}^{n_\lambda} \sum_{m=-2}^2 \langle |C_{\lambda i \vec{k}}^{dm}|^2 \rangle_{av},$$

$$\gamma = \int d\Omega_{\vec{k}} |(\phi_{c\vec{k}, x} | \nabla | \phi_{x, n_p})|^2 \times (\int d\Omega_{\vec{k}} |(\phi_{c\vec{k}, Cu} | \nabla | \phi_{Cu, 3d})|^2)^{-1}. \quad (8)$$

Here, abbreviated notations  $C_{\lambda i \vec{k}}^{pm}$  and  $C_{\lambda i \vec{k}}^{dm}$  mean

$C_{\lambda i \vec{k}}^{x, n, pm}$  and  $C_{\lambda i \vec{k}}^{Cu, 3dm}$ , respectively. The quantities  $p_\lambda$  and  $d_\lambda$  are the average fractions of the  $p$  and  $d$  components in the  $\lambda$  valence band.

In the eigenvalue problem for the tight-binding valence states, the Hamiltonian matrix elements are formed between the Bloch sums used in the expansion of  $\Psi_{\lambda i \vec{k}}$ . Because of the assumed orthonormality of the Bloch sums, the coefficient is given by the  $(\mu\alpha, \lambda i)$ th element of the  $8 \times 8$  unitary transformation matrix diagonalizing the Hamiltonian matrix. The unitary conditions are

$$\sum_{m=-1}^1 |C_{\lambda i \vec{k}}^{pm}|^2 + \sum_{m=-2}^2 |C_{\lambda i \vec{k}}^{dm}|^2 = 1 \quad (\lambda = u, l), \quad (9)$$

$$\sum_{i=1}^{n_u} |C_{u i \vec{k}}^{\xi m}|^2 + \sum_{i=1}^{n_l} |C_{l i \vec{k}}^{\xi m}|^2 = 1 \quad (\xi = p, d).$$

These directly give the mutual relations among the mixing rates:

$$p_u + d_u = 1, \quad p_l + d_l = 1, \quad (10)$$

$$n_u p_u + n_l p_l = 3, \quad n_u d_u + n_l d_l = 5.$$

If the ratio  $R$  is obtained from experimental spectrum and the value of  $\gamma$  is calculated from the ionic orbitals, all mixing rates can be evaluated from Eqs. (6) and (10) under an appropriate choice of  $n_u$  satisfying  $n_u + n_l = 8$ . The  $k$  dependence of  $\int d\Omega_{\vec{k}} |(\phi_{c\vec{k}, \mu} | \nabla | \phi_{\mu, \alpha})|^2$  is often important in optical problems. Handy expressions of the quantity are given in the Appendix.

In evaluating  $\gamma$  from Eqs. (8) and (A10), the Roothaan-Hartree-Fock wave functions calculated by Clementi<sup>14</sup> are used for  $\text{Cu}^+$ ,  $\text{Cl}^-$ , and  $\text{Br}^-$  orbitals. For the large value of  $k$ , the behaviors of wave functions near the nucleus are important. These wave functions are thought to be very close approximations to the exact Hartree-Fock wave functions not only in the high charge-density region, but also in the regions near and far from the nucleus. Since such a wave function is not available for  $\Gamma_1$ , the Hartree-Fock-Slater  $\Gamma_1 5p$  wave function, calculated by Kunz<sup>15</sup> by the method of Herman and Skillman,<sup>16</sup> is used for  $\text{CuI}$ , and the orthogonalization is omitted approximately. The values of  $\gamma$  for  $\text{MgK}_\alpha$  irradiation ( $k \approx 9.6$  a. u.) are 0.264, 0.035, and 0.258 for  $\text{CuCl}$ ,  $\text{CuBr}$ , and  $\text{CuI}$ , respectively. The small value of  $\gamma$  for  $\text{CuBr}$  is due to the fact that the value of  $k$  lies close to the second node of Fourier transform  $f_{4p}(k)$  of the  $\text{Br}^- 4p$  radial wave function ( $k \approx 9.3$  a. u.) accidentally, and thus the contribution arises mainly from the orthogonalization term [see Eqs. (A3) and (A10)]. Values of  $\gamma$  depend on the wave functions used. For example, the wave functions constructed by Slater's rule<sup>17</sup> with the correct number of nodes give much larger values of  $\gamma$ . This is mainly due to a wrong behavior of the  $\text{Cu}^+ 3d$  wave function

TABLE I. Fractions of the  $d$  components of the valence bands of cuprous halides.

	$d_l$	Average over the valence bands <sup>a</sup>			Cardona <sup>b</sup>	Values at the top of the valence band		
		$d_u$	$d_{u2}$	$d_{u1}$		Suga <i>et al.</i> <sup>c</sup>	Song <sup>d</sup>	Shindo <i>et al.</i> <sup>e</sup>
CuCl	0.24	0.86	1	0.76	0.75	$0.73 \pm 0.02$	0.79	0.56
CuBr	0.52	0.69	1	0.49	0.64	$0.57 \pm 0.03$	...	0.61
CuI	0.39	0.77	1	0.61	0.50	0.1 ~ 0.4	...	0.51

<sup>a</sup>Present work.<sup>b</sup>Reference 4.<sup>c</sup>Reference 18.<sup>d</sup>Reference 6.<sup>e</sup>K. Shindo, A. Morita, and H. Kamimura, J. Phys. Soc. Japan 21, 2748 (1966).

with a peak too small and too distant from the nucleus.

It is expected that the upper valence band is composed of five component bands, and the lower valence band three components. Thus,  $n_u=5$  and  $n_l=3$ . From the result shown in Fig. 2,  $R$  is estimated as 3.41, 2.16, and 2.51, for CuCl, CuBr, and CuI, respectively. The substitution of the values of  $R$  and  $\gamma$  given above into Eqs. (6) and (10) yields the values of  $d_u$  and  $d_l$  shown in Table I. This result shows that the upper valence band is  $d$  rich. Another possible choice that  $n_u=3$  and  $n_l=5$  leads to unphysical values of  $d_u$ , for example, 1.67 for CuCl and 1.17 for CuBr.

As is obvious in Fig. 2, the upper and lower bands have structures. If the structures arise from the admixture of component bands, the procedure for the evaluation of the  $p$ - $d$  mixing rates described above will also be applicable to these component bands. According to Song's band calculation,<sup>6</sup> the result of which is illustrated in Fig. 4, the upper valence band may possibly have component bands. One of the components contains the  $\Gamma_{15}$  state. The other containing the  $\Gamma_{12}$  state is of almost pure  $d$ -type symmetry. Equations analogous to Eqs. (6) and (10) are obtained as

$$R' = 3(\gamma p_{u1} + d_{u1}) / 2(\gamma p_{u2} + d_{u2}),$$

$$p_{u1} + d_{u1} = p_{u2} + d_{u2} = 1,$$

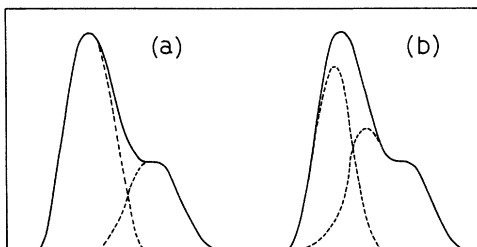


FIG. 3. Decomposition of the upper valence band of CuCl. (a) Simple decomposition. (b) Decomposition expected from the estimation of the average  $p$ - $d$  mixing rates for the subbands, under the assumption of the pure  $d$ -type lower subband.

$$3p_{u1} + 2p_{u2} = 5p_u, \quad 3d_{u1} + 2d_{u2} = 5d_u. \quad (11)$$

Subscripts 1 and 2 distinguish the upper and lower components, respectively, and  $\gamma$ ,  $p_u$ , and  $d_u$  are the same as before.

If the upper band is decomposed simply as illustrated in Fig. 3(a), the estimated values of  $R'$  are 0.45, 0.48, and 0.65 for CuCl, CuBr, and CuI, respectively. With these values and Eq. (11), the values of  $d_{u2}$  are evaluated to be 1.7, 1.2, and 1.3 for CuCl, CuBr, and CuI, respectively. These values are all larger than unity and meaningless. The origin for this may be the wrongly estimated value of  $R'$ . The width of the lower subband of almost pure  $d$  type may be narrower than that shown in Fig. 3(a).<sup>6</sup> Since the decomposition of the upper band can not be made uniquely, we will not try to decompose the upper band in such a manner. Alternatively, we assume that  $d_{u2}=1$  because of the almost pure  $d$ -type nature of the lower subband. The values of  $d_{u1}$  thus obtained from Eq. (11) are tabulated in Table I. The corresponding values of  $R'$  are 1.24, 0.75, and 1.06 for CuCl, CuBr, and CuI, respectively. In order that the value of  $d_{u2}$  is smaller than unity, the values of  $R'$  should be larger than those given above. These values of  $R'$  suggest that the decomposition of the upper band should rather be altered like that shown in Fig. 3(b). The lower subband in Fig. 3(b) is narrower than that in Fig. 3(a).

The  $p$ - $d$  mixing rate at the top of the valence band can be estimated by other methods. The values reported so far are cited in Table I for comparison. The values by Suga *et al.*<sup>18</sup> are obtained from the analysis of the effective  $g$  values of the exciton band in the Faraday rotation spectra, and all others<sup>4-6</sup> are based on the analysis of the spin-orbit splitting of the exciton absorption band. Although the average  $p$ - $d$  mixing rate is different in its definition from that at the top of the valence band, the values of  $d_{u1}$  obtained here are in fair agreement with the values obtained by others. The value for CuI obtained by Suga *et al.* appears to be too small as compared with others. The origin of this disagreement is not clear at present. The

average fraction  $d_u$  of the  $d$  component in the upper band is larger than that at the top of the valence band. The almost pure  $d$ -type subband involving the  $\Gamma_{12}$  state gives a substantial contribution to this.

### V. DISCUSSION

There are some optical phenomena which are closely related to the density of states of the valence band as the x-ray photoemission. They are the fundamental absorption, the soft-x-ray emission, and UPS. They have already been measured on cuprous halides, and are compared with the present result in Figs. 4 and 5. Figure 4 shows, for the case of CuCl, the spectra of the  $\text{Cu}^+L_\alpha$  emission,<sup>19</sup> the  $\text{Cl}^-L_{2,3}$  emission,<sup>20</sup> the UPS optical density of states obtained under the assumption of the constant transition matrix element,<sup>21</sup> and the

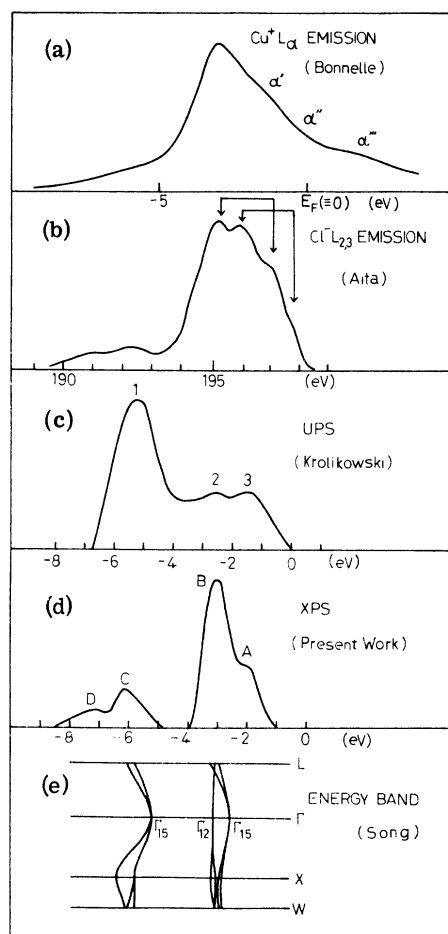


FIG. 4. Comparison of the valence-band spectra of CuCl obtained by various optical measurements. (a) Copper  $L_\alpha$  emission spectrum. (b) Chlorine  $L_{2,3}$  emission spectrum. (c) Optical density of states estimated from the ultraviolet photoemission spectrum. (d) Present XPS spectrum. (e) Energy-band structure calculated by Song.

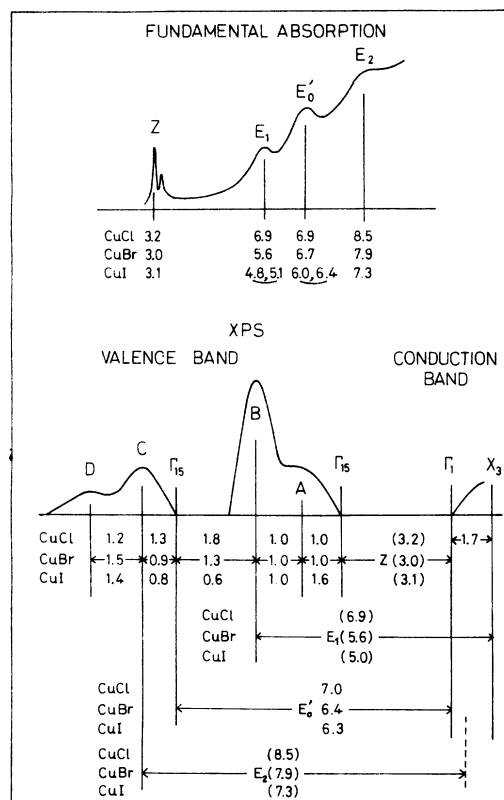


FIG. 5. Schematic illustration of the relation between the energies of the characteristic points in the XPS spectra and the fundamental absorption spectra. Values in parentheses are taken from the energies of the peak positions in the fundamental absorption spectra. Units are all in eV.

x-ray photoemission. The energy-band structure calculated by Song<sup>6</sup> is also shown. The  $\text{Cu}^+L_\alpha$  emission spectrum originates from the transition of a valence electron to the  $2p$  hole in the  $\text{Cu}^+$  ion. The structures occurring on the high-energy side of the main band, which are denoted as  $\alpha'$ ,  $\alpha''$ , and  $\alpha'''$ , are the satellites due to multiple ionization. The electronic transition in the  $\text{Cl}^-L_{2,3}$  emission occurs to the  $2p$  hole in the  $\text{Cl}^-$  ion. The structures in the spectrum are doubled owing to the spin-orbit splitting of the  $2p$  level. The spin-orbit partners are shown by linked arrows in the figure.

All of the spectra shown in Fig. 4 show a common aspect that the valence band of CuCl is composed of two branches. The over-all resolution of the soft-x-ray emission spectrum for the analysis of the energy-band structure appears to be inferior to that of the photoemission. The disagreement of the profiles among various spectra may be due to the difference of the transition matrix elements. For example, the  $\text{Cl}^-L_{2,3}$  transition includes the transfer of an electron from a copper ion to a chlo-

rine ion with a hole in the core state. In the case of the UPS spectrum, the energy and momentum dependence of the transition matrix element may be important, since the transition occurs to the states near the bottom of the conduction band.

Three peaks are observed in the optical density of states estimated from the UPS spectrum. Peaks 1, 2, and 3 in the UPS spectrum correspond well to the peaks C, B, and A in the XPS spectrum, respectively. No peak corresponding to the peak D in the XPS spectrum is observed in the UPS spectrum. This may be ascribed to the low excitation energy in the case of the UPS experiment. The forbidden band between the upper and lower valence bands is not observed in the spectrum of the UPS optical density of states. The spectrum of inelastically scattered electrons inevitably overlaps the valence-band spectrum in the case of UPS. Even if a certain correction for this is made, there still remains a possibility of this effect to mask the existence of a forbidden band. The UPS spectra have also been measured on CuBr and CuI.<sup>21</sup> The relations between the XPS and UPS spectra of CuBr and CuI are found to be similar to that of CuCl. Thus, the UPS and XPS results are qualitatively in good agreement. They are also compatible, at least qualitatively, with the result of Song's band calculation.

The fundamental absorption spectra in the ultraviolet region should be interpreted consistently with the XPS spectra obtained here. One of the characteristic aspects of the fundamental absorption spectra is that the absorption intensity is weak near the threshold. In the cases of CuCl and CuBr,<sup>3</sup> for example, the threshold is located around 3 eV and intensity is weak below 7 eV. Such a feature is consistent with the present result that the major part of the upper valence band arises from the *d*-type states, since most of the low-energy part of the conduction band are composed of the *s*-type states. In Fig. 5 energy separations between various characteristic points in the XPS spectra are summarized. The values of the energy separations for CuCl, CuBr, and CuI are given below the XPS spectrum in that order. The energies of the peak positions observed by Ishii *et al.*<sup>3</sup> for CuCl and CuBr and by Cardona<sup>4</sup> for CuI are also shown in the figure. The nomenclature is after Cardona. It should be noted that the  $E_1$  and  $E'_0$  peaks overlap each other in CuCl and only a single peak is observed around 6.9 eV. The decomposition of this band into components can not be carried out without serious ambiguity. The energy of the lowest exciton band is taken as the band-gap energy, since the exciton binding energy is too small as compared with the accuracy involved in the argument described below.

As is obvious in Fig. 5, the energies of the  $E'_0$

peaks, 6.9, 6.7, and 6.0~6.4 eV for CuCl, CuBr, and CuI, respectively, are roughly equal to the values of the separations, 7.0, 6.4, and 6.3 eV, between the top of the lower valence band and the bottom of the conduction band in the respective materials. Therefore, the  $E'_0$  peak will be assigned to the transition from the top of the lower valence band to the bottom of the conduction band ( $\Gamma_{15} \rightarrow \Gamma_1$ ). Perhaps, this transition results in a formation of an exciton. This exciton state occurs in energy in the region of the continuous absorption due to the transition from the upper valence band. In a case like this, the exciton produced may have a large probability of the autoionization to decompose into a pair of a free electron and a free hole, and have a short lifetime. As a result, the observed exciton line is much more broadened than the ordinary exciton line at the threshold of the fundamental absorption. This will explain the difference of the width between the exciton band at the threshold and the  $E'_0$  band. If the background due to overlapping continuous absorption is subtracted appropriately, the integrated intensity of the  $E'_0$  band is estimated. It is found for CuCl that the integrated intensity of the  $E'_0$  band is roughly ten times as large as those of the *Z* exciton bands. This ratio is not too large as compared with the ratio 5:1 of the fraction of the *p* components of the lower valence band to that of the upper valence band.

The energies of the  $E_1$  peaks in CuBr and CuI are smaller than the separations between the lower valence band and the bottom of the conduction band. Therefore, the  $E_1$  band must be caused by the transition from the upper valence band. A tentative assignment of the  $E_1$  band is to the transition from the states corresponding to the most intense peak B in the upper band. Since the majority of the states around the peak B are of *d*-type, the states of the conduction band responsible for the transition should be of *p* type. Thus, an electron may be excited to a state near the  $X_3$  point, around which a plenty of *p*-type states may be contained. Since the peak  $E_1$  and the peak  $E'_0$  occur at nearly the same energy in CuCl, the separation between the top of the lower valence band and the peak B should be equal to the separation between the  $\Gamma_1$  and  $X_3$  points in the conduction band in this material. According to the recent band calculation by Kahn,<sup>22</sup> the separation between the  $\Gamma_1$  and  $X_3$  points is 1.7 eV, and agrees well with the separation 1.8 eV between the top of the lower band and the B peak. According to this assignment, the energy separation between the  $\Gamma_1$  and  $X_3$  points in the conduction band of CuBr is about 0.6 eV and fairly smaller than that of CuCl. The value for CuI is negative and the assignment should be altered for this material.

The assignment of the  $E_2$  peak can not be made without more ambiguity. We tentatively assign the  $E_2$  peak to the transition between the states around the peak C in the lower band to the states near the bottom of the conduction band, because the energy responsible for the transition is roughly equal to the energy at the  $E_2$  peak.

#### ACKNOWLEDGMENTS

The authors wish to thank Professor W. E. Spicer for sending a copy of Dr. Krolikowski's thesis, Professor M. Ueta and his colleagues for supplying samples, Professor A. Morita for discussion on the theoretical part, Dr. I. Nagakura and S. Suzuki for the computer work, and Dr. O. Aita for sending the soft-x-ray data prior to publication. The present work has been financially supported by the Grant-in-Aid from the Ministry of Education.

#### APPENDIX

Expressions for  $\int d\Omega_{\vec{k}} |\phi_{\sigma\vec{k},\mu} | \vec{A} | \phi_{\mu,\alpha} |^2$ , where  $\vec{A} = \nabla$  or  $\vec{r}$ , with SOPW

$$\phi_{\sigma\vec{k},\mu}(\vec{r}) = N_{\sigma\vec{k}} \left[ \Omega_0^{-1/2} e^{i\vec{k}\cdot\vec{r}} - \sum_{\alpha'} B_{\vec{k},\mu\alpha'} \phi_{\mu,\alpha'}(\vec{r}) \right] \quad (\text{A1})$$

are given in handy forms. In Eq. (A1) the orthogonalization coefficient  $B_{\vec{k},\mu\alpha}$  can be written from a variable-separated form of  $\phi_{\mu,\alpha}(\vec{r}) = R_{\mu,nl}(r) \times Y_{lm}(\Omega_{\vec{r}})$  as

$$B_{\vec{k},\mu\alpha} = 4\pi \Omega_0^{-1/2} i^l f_{\mu,nl}(k) Y_{lm}^*(\Omega_{\vec{k}}), \quad (\text{A2})$$

$$f_{\mu,nl}(k) = \int_0^\infty r^2 R_{\mu,nl}(r) j_l(kr) dr, \quad (\text{A3})$$

$Y_{lm}$  and  $j_l$  are the spherical harmonics and the spherical Bessel function, respectively. The subscripts  $c$  and  $\mu$ , the normalization constant  $N_{\sigma\vec{k}}$ , and unit cell volume  $\Omega_0$  will be dropped in what follows.

Consider the following expressions:

$$(e^{i\vec{k}\cdot\vec{r}} | A_{\xi} | \phi_{nlm}) = 4\pi (-i)^{l-1} [Y_{l-1,m+\sigma}(\Omega_{\vec{k}}) a_{-}(lm; 1\sigma) \langle j_{l-1} | D_{l+1} | R_{nl} \rangle - Y_{l+1,m+\sigma}(\Omega_{\vec{k}}) a_{+}(lm; 1\sigma) \langle j_{l+1} | D_{-l} | R_{nl} \rangle], \quad (\text{A4})$$

$$(\phi_{n'l'm'} | A_{\xi} | \phi_{nlm}) = [a_{-}(lm; 1\sigma) \langle R_{n',l-1} | D_{l+1} | R_{nl} \rangle \delta_{l',l-1} + a_{+}(lm; 1\sigma) \langle R_{n',l+1} | D_{-l} | R_{nl} \rangle \delta_{l',l+1}] \delta_{m',m+\sigma}. \quad (\text{A5})$$

Here  $A_{\xi} = A_{\pm} [= (A_x \pm iA_y)/\sqrt{2}]$  or  $A_z$ ,  $\sigma = 1, 0, -1$  for  $\xi = +, z, -$ , respectively, and  $\langle f | D_j | g \rangle = \int_0^\infty r^2 f D_j g dr$  with  $D_j = d/dr + j/r$  for  $\vec{A} = \nabla$  and with  $D_j = r$  for  $\vec{A} = \vec{r}$ .  $a_{\pm}(lm; 1\sigma)$  are the coefficients introduced by the expansion of  $Y_{lm} Y_{l\sigma}$  in terms of  $Y_{l\pm 1, m\sigma}$  and are given by

$$a_{\pm}(lm; 1\sigma) = [2(2l \pm 1)(2l + 2 \pm 1)]^{-1/2} \times \begin{cases} (-1)^{1/2 \pm 1/2} [(l \pm m \pm 1)(l \pm m + 1 \pm 1)]^{1/2} & (\sigma = 1) \\ [2(l + m + \frac{1}{2} \pm \frac{1}{2})(l - m + \frac{1}{2} \pm \frac{1}{2})]^{1/2} & (\sigma = 0) \\ (-1)^{1/2 \mp 1/2} [(l \mp m \pm 1)(l \mp m + 1 \pm 1)]^{1/2} & (\sigma = -1) \end{cases} \quad (\text{A6})$$

and are zero for negative argument of the square roots. They have the properties

$$a_{\mp}(l \pm 1, m + \sigma; 1, -\sigma) = a_{\pm}(lm; 1\sigma), \quad (\text{A7})$$

$$\sum_{\sigma=-1}^1 [a_{\pm}(lm; 1\sigma)]^2 = (l + \frac{1}{2} \pm \frac{1}{2}) / (2l + 1).$$

From Eqs. (A1)–(A7) one can obtain (again,  $\vec{A} = \nabla$  or  $\vec{r}$ )

$$\int d\Omega_{\vec{k}} |\phi_{\vec{k}} | \vec{A} | \phi_{nlm}|^2 / (4\pi)^2 = (2l+1)^{-1} \{ l [ \langle j_{l-1}(kr) | D_{l+1} | R_{nl} \rangle - F_{l-1, nl}^{(l+1)}(k) ]^2 + (l+1) [ \langle j_{l+1}(kr) | D_{-l} | R_{nl} \rangle - F_{l+1, nl}^{(l-1)}(k) ]^2 \}, \quad (\text{A8})$$

where

$$F_{l', nl}^{(j)}(k) = \sum_{n'} \langle R_{n', l'} | D_j | R_{nl} \rangle f_{n', l'}(k). \quad (\text{A9})$$

By operating  $\nabla$  to SOPW  $\phi_{\vec{k}}$ , an expression which is explicitly connected with the Fourier transforms of radial wave functions  $f_{nl}(k)$ 's, is obtained as

$$\int d\Omega_{\vec{k}} |\phi_{\vec{k}} | \nabla | \phi_{nlm}|^2 / (4\pi)^2 = k^2 f_{nl}^2(k) - 2(2l+1)^{-1} k f_{nl}(k) \times [l F_{l-1, nl}^{(l+1)}(k) - (l+1) F_{l+1, nl}^{(l-1)}(k)] + (2l+1)^{-1} \times \{ l [F_{l-1, nl}^{(l+1)}(k)]^2 + (l+1) [F_{l+1, nl}^{(l-1)}(k)]^2 \}. \quad (\text{A10})$$

<sup>1</sup>S. Kono, T. Ishii, T. Sagawa, and T. Kobayasi, Phys. Rev. Lett. **28**, 1385 (1972).

<sup>2</sup>F. Herman, J. Electron. **1**, 103 (1955).

<sup>3</sup>T. Ishii, S. Sato, T. Matsukawa, Y. Sakisaka, and T. Sagawa, J. Phys. Soc. Jap. **32**, 1440 (1972).

<sup>4</sup>M. Cardona, Phys. Rev. **129**, 69 (1963).

<sup>5</sup>K. Shindo, A. Morita, and H. Kamimura, J. Phys. Soc. Jap.

**20**, 2054 (1965).

<sup>6</sup>K. S. Song, J. Phys. Chem. Solids **28**, 2003 (1967).

<sup>7</sup>F. Herman and D. S. McClure, Bull. Am. Phys. Soc. **5**, 48 (1960).

<sup>8</sup>Electron Spectroscopy, edited by D. A. Shirley (North-Holland, Amsterdam, 1972).

<sup>9</sup>M. Ueta and T. Goto, J. Phys. Soc. Jap. **20**, 401 (1965).

- <sup>10</sup>T. Novakov, Phys. Rev. B **3**, 2693 (1971); T. Novakov and R. Prin, in Ref. 8, p. 821.
- <sup>11</sup>D. C. Frost, A. Ishitani, and C. A. McDowell, Mol. Phys. **24**, 861 (1972).
- <sup>12</sup>Y. Baer, P. E. Hedén, J. Hedman, M. Klasson, C. Nordling, and K. Siegbah, Phys. Scr. **1**, 55 (1970).
- <sup>13</sup>P. A. Jansson, J. Opt. Soc. Am. **60**, 184 (1970).
- <sup>14</sup>E. Clementi, IBM J. Res. Develop. Suppl. **9**:2 (1965).
- <sup>15</sup>A. B. Kunz, Phys. Rev. **151**, 620 (1966).
- <sup>16</sup>F. Herman and S. Skillman, *Atomic Structure Calculations* (Prentice-Hall, Englewood Cliffs, N. J., 1963).
- <sup>17</sup>J. C. Slater, Phys. Rev. **36**, 57 (1930).
- <sup>18</sup>S. Suga, T. Koda, and T. Mitani, Phys. Status Solidi **48**, 753 (1971).
- <sup>19</sup>C. Bonnelle, J. Phys. (Paris) **28**, 3 (1967).
- <sup>20</sup>O. Aita, J. Phys. Soc. Jap. **34**, 1112 (1973).
- <sup>21</sup>W. F. Krolikowski, thesis (Stanford University, 1967) (unpublished).
- <sup>22</sup>M. A. Kahn, Solid State Commun. **11**, 587 (1972).

PHYSICAL REVIEW B

VOLUME 8, NUMBER 2

15 JULY 1973

## Carrier Generation Processes in Poly(*N*-Vinylcarbazole) Films

P. J. Reucroft and S. K. Ghosh

*Department of Metallurgical Engineering and Materials Science, University of Kentucky, Lexington, Kentucky 40506*

(Received 14 February 1972; revised manuscript received 9 February 1973)

Studies on the conductivity and photoconductivity of amorphous films of poly (*N*-vinylcarbazole) with SnO<sub>2</sub> and metal electrodes show that the dark conductivity is dominated by the Richardson-Schottky field-assisted hole emission from positively biased metal electrodes, provided the metal work function is greater than 3.8 eV. When the metal electrode is negatively biased or with lower-work-function electrodes, the conductivity appears to be dominated by a bulk-polymer-film effect. The current-voltage characteristics of the latter effect do not support a Poole-Frenkel process. High-work-function metal electrodes in positive bias give rise to hole-photoemission tails in the photocurrent-action spectrum. A photocarrier generation process, which onsets at 1.8–1.9 eV and obscures hole photoemission from low-work-function metal electrodes, produces a linear dependence of photocurrent on light intensity and appears to be associated with electronic transitions in the polymer film.

### INTRODUCTION

A considerable amount of progress has been made in understanding photoconductivity and semi-conductivity phenomena in organic crystals in recent years.<sup>1</sup> The situation with regard to understanding similar phenomena observed in organic polymers is less satisfactory. This can be largely attributed to the greater difficulties in obtaining well-characterized samples and the semi- or non-crystalline nature of polymer specimens. The increasing importance of polymeric materials in electrophotography and recent emphasis on the electronic properties of amorphous materials in general has, however, stimulated a renewal of interest in both carrier generation and transport in polymers. Carrier mobilities have been reported in poly (*N*-vinylcarbazole)<sup>2</sup> (PVK), polyvinylchloride,<sup>3</sup> and other polymers.<sup>4</sup> Photoinjection of carriers through electrodes<sup>5</sup> and photocarrier generation via excitons<sup>6</sup> have also been investigated. Progress has been made in understanding mechanisms of spectral sensitization in poly(*N*-vinylcarbazole).<sup>7</sup>

Recent studies on photoinjected space-charge-perturbed currents in PVK films are particularly intriguing because they indicate that deep carrier trapping may not be a major problem in relatively

uncharacterized amorphous materials in contrast to the situation that obtains in the case of organic molecular single crystals.<sup>2(e)</sup> These findings, in conjunction with hole-photoemission studies on metal-PVK-SnO<sub>2</sub> samples,<sup>5(a)</sup> indicate that the dark-conduction mechanism is likely to be dominated by the Richardson-Schottky field-assisted thermionic hole emission. To determine the extent to which this mechanism is operative and also gain additional information on photocarrier generation in amorphous PVK, steady-state-photoconductivity and dark-conductivity measurements have been carried out on metal-PVK-SnO<sub>2</sub> samples with metals having work functions in the range 3.8–6.3 eV.

### EXPERIMENTAL TECHNIQUES

Optically clear PVK films were cast evenly on the conducting side of ultrasonically clean Nesa glass from a solution consisting of 17% PVK, 17% cyclohexanone, and 66% toluene by weight. The sample was placed in a saturated atmosphere of the solvent 1:4 (cyclohexanone-toluene) for 4–5 h then dried at (35–70) °C, for 4–8 h. A metal film (thickness 800 Å; area 5–6 cm<sup>2</sup>) was vacuum evaporated onto the PVK to complete the electrode system. The PVK film thicknesses were determined by capacitance measurements to be 30 ± 5 μ.

The experimental arrangement used for the pho-